Check for updates

Improved localized mRNA delivery using lipid nanoparticles with a novel synthetic cholesterol derivative

Deepak K. Sahel,[a] Jonas Renner,[a] Kseniia Yu. Vlasova,[a] Nathan D. Pennock,[b] Sakib T. Haque, [ID] [a] Antony Jozic,[a] Joshua M. Walker,[b,e,f] Conroy Sun [ID] [a,b,d] and Gaurav Sahay [ID] *[a,c,d]

Lipid nanoparticles (LNPs) are self-assembled nanocarriers made up of ionizable cationic lipids, membrane lipids, sterols, and PEGylated lipids in a predetermined proportion to encapsulate nucleic acid payloads. According to recent findings, following local administration (intramuscular, intratumoral), LNPs diffuse into the systemic circulation and subsequently show liver transfection. Liver transfection can result in both liver toxicity and undesirable cargo distribution. To address this issue, we synthesized a novel cholesterol derivative, glutamate–cholesterol (GA–Chol), which, when incorporated in LNPs (GA–Chol LNPs), improved *in vitro* transfection efficiency by approximately 10-fold and 20-fold in HEK293T and HeLa cells, respectively. Furthermore, when GA–Chol LNPs were injected intramuscularly or intratumorally, robust localized transfection was observed in either the injected muscle or the flank tumors, without significant transfection in the liver. This observation was consistent across multiple cell lines, representing various types of cancer. Leverage local delivery strategy, mRNA encoding for constitutively active caspase-3 was encapsulated with GA–Chol LNPs and delivered intratumorally in 4T1 tumor-bearing BALB/c mice, resulting in a significantly reduced and sustained tumor burden. Overall, these findings describe the potential application of a synthetic cholesterol derivative for the localized transfection of LNPs.

1. Introduction

Lipid nanoparticles (LNPs) are an extremely promising non-viral vector for mRNA delivery applications.[1] The clinical success of LNPs is evident in the COVID-19 vaccines from Pfizer-BioNTech (BNT162b2) and Moderna (mRNA-1273), which have the brand names Comirnaty® and Spikevax®, respectively.[2] Moreover, more than 80 LNPs-based gene drugs have entered clinical development.[3] LNPs are comprised of four major components: ionizable cationic lipids to condense nucleic acids, membrane lipids as helper lipids, cholesterol to stabilize particles, and PEG lipids to provide a stealth effect

and aid in self-assembly.[4] While all four components play a significant role in the self-assembly of LNPs to encapsulate nucleic acid, the ionizable cationic lipids are the most frequently tested component to improve LNPs' characteristics and efficiency. However, cholesterol is one of the key components present in both the outer shell (solute-facing) and the inner core of LNPs.[5] Prior reports have explored the significant role of cholesterol in membrane fusion, endosomal escape, and nanoparticle trafficking, resulting in impacts on overall mRNA transfection efficiency and functional efficacy.[6] Moreover, it has been reported that the cholesterol in LNPs can be recognized by an enzyme called Niemann-Pick C1 (NPC1), which leads to the endosomal recycling of ~70% of the total endocytosed nucleic acid.[7] Likewise, prior reports of chemical modifications of cholesterol to make cationic cholesterol (for example, 3β-[*N*-(*N*′,*N*′-dimethylaminoethane)-carbamoyl] cholesterol hydrochloride (DC–Chol)) demonstrated altered LNP properties conferring non-hepatic (lung) benefits in mRNA delivery.[8]

Typically, after systemic administration, conventional LNPs are subject to protein corona formation, including binding to apolipoprotein E (ApoE). The presence of ApoE on LNPs then facilitates LNP internalization into hepatocytes *via* low-density lipoprotein receptor (LDLR)-mediated endocytosis.[9–11]

[a]Department of Pharmaceutical Sciences, College of Pharmacy, Robertson Life Sciences Building, Oregon State University, Portland, OR 97201, USA. E-mail: sahay@ohsu.edu

[b]Department of Radiation Medicine, School of Medicine, Oregon Health & Science University, Portland, OR, USA

[c]Department of Biomedical Engineering, Robertson Life Sciences Building, Oregon Health & Science University, Portland, OR, USA

[d]Center for Innovative Drug Delivery and Imaging, College of Pharmacy, Oregon State University & Oregon Health & Science University, Portland, OR, USA

[e]Department of Cell, Developmental, and Cancer Biology, School of Medicine, Oregon Health & Science University, Portland, OR, USA

[f]Knight Cancer Institute, Oregon Health & Science University, Portland, OR, USA

Multiple studies have shown that LNPs injected through a local route (*i.e.*, intramuscularly) rapidly enter the systemic circulation and accumulate in the liver.[12–16] The liver-tropic behaviors of most LNPs limit their therapeutic applications and can also lead to hepatotoxicity. One such example has been reported with the Comirnaty® vaccine, which, when injected intramuscularly, has been reported to cause liver injury as an off-target effect or side effect.[5,17] Likewise, LNPs injected directly into the tumor also have a high risk of off-target hepatotoxicity clinically.[5] Therefore, a rational approach is required to facilitate the extrahepatic delivery of LNPs, especially when intended for local delivery and cargo expression.

Herein, we report a novel synthetic derivative of cholesterol, namely glutamate–cholesterol (GA–Chol), which was synthesized by covalently conjugating glutamic acid to cholesterol. We have previously reported that replacing cholesterol with β-sitosterol alters the morphology of LNPs to a polyhedral shape and significantly enhances transfection efficiency *in vitro*.[18–20] Here, we hypothesized that conjugating cholesterol with glutamic acid can alter its physiological properties and modulate the behavior of LNPs. Cholesterol was replaced with GA–Chol, and the LNPs were prepared and tested *in vitro* for transfection efficiency. This was followed by *in vivo* screening after systemic and local administration. We found that the GA–Chol LNPs accumulated at the site of injection and did not result in hepatic expression after intramuscular or intratumoral injections *in vivo* in mice. Therapeutically, constitutively active caspase-3 mRNA encapsulated into GA–Chol LNPs, when injected into established 4T1 orthotopic breast tumor-bearing mice, demonstrated a significant reduction in tumor burden, followed by prolonged tumor burden stasis.

2. Materials and methods

2.1. Materials

D-Lin–MC3–DMA lipid was purchased from BroadPharm, 1,2-distearoyl-*sn-glycero*-3-phosphocholine (DSPC) was purchased from Avanti Polar Lipids, cholesterol was purchased from Thermo Scientific, and DMG–PEG2k was purchased from NOF America Corporation. Quant-iT™ RiboGreen Reagent and RNA Assay Kit, dimethyl ʟ-glutamate hydrochloride, and Triphosgene were purchased from Thermo Scientific. All the solvents were of HPLC grade and purchased from Thermo Scientific. Firefly Luciferase mRNA (FLuc mRNA (N1MePU)) was purchased from Helix Biotech, Inc., and constitutively active caspase-3 mRNA was custom-synthesized by Helix Biotech, Inc.

2.2. Methodology

2.2.1. Synthesis and characterization of GA–Chol. A synthesis scheme for GA–Chol is shown in Fig. 1a. Briefly, 47.25 mmol of dimethyl ʟ-glutamate hydrochloride (1) and 15.59 mmol of Triphosgene were taken in a round-bottom flask and dissolved in 250 mL of dichloromethane, followed by

cooling down at −78 °C under a N_2 atmosphere. Further, 103.95 mmol of triethylamine was added dropwise to the reaction mixture and stirred for 1 h at −78 °C. Next, the reaction was allowed to warm to room temperature while stirring for another hour. The solvent was removed under reduced pressure, and the crude residue was filtered through a Celite plug to yield an intermediate product, namely dimethyl (*S*)-2-isocyanatopentanedioate (**2**), as a colorless oil, which was then used in the next step. Briefly, 12.92 mmol of dimethyl (*S*)-2-isocyanatopentanedioate (**2**) and 14.22 mmol of cholesterol were dissolved in 50 mL of toluene in a round-bottom flask. The reaction was refluxed at 130 °C for 5 h under an N2 atmosphere. Further, the solvent was removed under reduced pressure, and the obtained product was recrystallized in methanol to obtain a purified dimethyl glutamate–cholesterol conjugate (**3**). Finally, the dimethyl glutamate–cholesterol conjugate was saponified using potassium hydroxide in a methanolic solution to yield glutamate–cholesterol conjugate (**3**).

2.2.2. LNPs preparation and characterization. All the lipids, including D-Lin–MC3–DMA/DSPC/Chol/DMG–PEG2k, were mixed thoroughly in ethanol in a mol% ratio of 50 : 10 : 38.5 : 1.5, respectively, and a lipid to mRNA ratio (wt : wt) of 20 : 1. The lipid solution was combined with an aqueous phase containing citrate buffer (25 mM, pH 4.0) and FLuc–mRNA using the NanoAssemblr™ (Precision NanoSystems) with a ratio of 1 : 3 (ethanol : aqueous) and a total flow rate of 9 mL min⁻¹. For GA–Chol LNP preparation, the GA–Chol was mixed in the aqueous phase instead of ethanol. The obtained LNPs were diluted 1 : 1 (v/v) with phosphate-buffered saline (PBS, pH 7.4) and added to a 10 kDa Slide-A-Lyzer dialysis bag to dialyze against pre-cooled PBS (pH 7.4) overnight at 4 °C. The GA–Chol LNPs were dialyzed for 2–3 h only. Furthermore, the LNPs were concentrated using a 10 kDa Amicon Ultra-4 mL centrifugal filter unit (Millipore, Burlington, MA) and evaluated for particle size and polydispersity index (PDI) using Stunner (Unchained Labs, Pleasanton, CA), and zeta potential using Dynamic Light Scattering (DLS) in the Zetasizer Nano ZS (Malvern Panalytical Inc., Westborough MA). The Quant-iT RiboGreen RNA reagent kit (Thermo Fisher Scientific, Waltham, MA) was then used to estimate encapsulation efficiency (%) and mRNA concentration. The LNPs were cryofrozen on a copper lacey carbon film-coated cryo-EM grid (Quantifoil, R1.2/1.3 300 Cu mesh) using a Vitrobot Mark IV system (FEI) and observed under Cryogenic Electron Microscopy (cryo-EM) assisted with Falcon III and K3 Summit cameras with a direct electron detector (DED) at 300 kV.

The mol% of GA–Chol was reduced to 20% to study how GA–Chol content affects localized transfection. The lipid composition was 50 : 28.5 : 20 : 1.5 mol% of D-Lin–MC3–DMA/DSPC/GA–Chol/DMG–PEG2k, respectively, and GA–Chol LNPs were prepared and characterized as described above.

2.2.3. *In vitro* studies. HEK293T, HeLa, HEK293T–Gal8–GFP, and TUBO cells were maintained in DMEM media, 4T1 and MCA-205 cells were maintained in RPMI-1640 media, and Yumm1.7 cells were maintained in DMEM:F12 media, all with
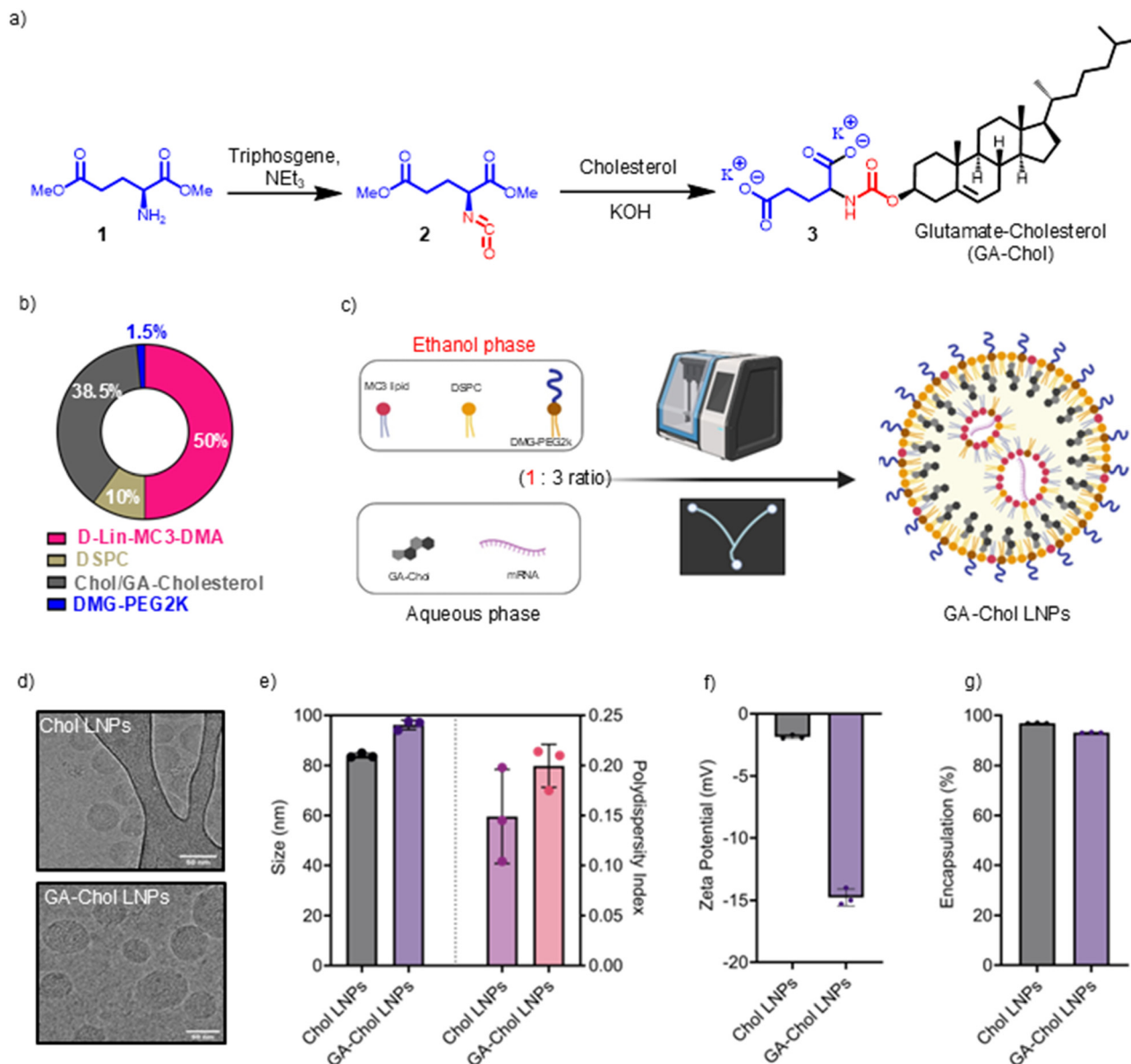
Fig. 1 (a) Synthesis scheme for GA–Chol, (b) lipid composition (mol%) of Chol/GA–Chol LNPs, (c) illustration of GA–Chol LNPs preparation using microfluidic device, (d) cryoEM images of Chol and GA–Chol LNPs, (e) particle size (nm) and polydispersity index, (f) encapsulation efficiency (%), and (g) zeta potential (mV) of Chol and GA–Chol LNPs. Data are presented as mean $\pm$ SEM (n = 3).

10% FBS and 1% pen/strep, and incubated at 37 °C with 5% CO_2 in a humid environment in a CO_2 incubator. The cells were passaged when they reached >70% confluency.

2.3.1. Transfection assay. HeLa or HEK293T cells were seeded in a 96-well plate at a density of 4×10^3 cells per well and allowed to grow overnight. The next day, the cells were treated with 50 ng, 100 ng, and 200 ng of FLuc mRNA containing Chol or GA–Chol LNPs, followed by a 24 h incubation. An equal volume of PBS was added to the wells of the negative control group. The transfection assay was performed using the ONE-Glo™ + Tox Luciferase Reporter and Cell Viability Assay kit (Promega Corporation, USA). Briefly, the cells were treated with Cell Titer reagent, and the fluorescence readings were

taken at Ex 485 nm and Em 510 nm. Further, ONE-Glo™ was added to the cells, and luminescence readings were taken using an Infinite® 200 PRO plate reader (Tecan, Switzerland). The transfection efficiency was calculated and plotted as normalized transfection (relative fluorescence/luminescence units, RFU/RLU).

2.3.2. Endosomal escape. We adopted a previously reported method to evaluate the endosomal escape of LNPs.[19] HEK293T–Gal8–GFP cells were plated in a 12-well plate (μ-Slide, Ibidi USA, Inc., Fitchburg, WI) with a density of 2×10^4 cells per well and allowed to adhere overnight. The next day, the cells were treated with 200 ng of FLuc mRNA containing Chol or GA–Chol LNPs, followed by a 24 h incubation.

Afterwards, the cells were fixed with 4% paraformaldehyde, stained with DAPI, and covered with a coverslip; they were then imaged using confocal microscopy (Leica DMi8, Leica Microsystems).

2.3.3. *In vitro* anticancer activity of caspase-3 mRNA. Briefly, 4T1 cells were seeded at a density of 3500 cells per well in 200 µL of complete media and were pipetted into a 96-well flat-bottom tissue culture-treated plate (Celltreat, 229196), evenly suspended, and then placed into the incubator overnight. The following day, the media and unattached cells were removed and replaced with fresh complete media. Cells were then treated with vehicle or LNPs containing 25, 50, or 100 ng of either FLuc mRNA, constitutively active caspase-3 mRNA, or the pan-kinase inhibitor Staurosporine (100 ng per well), as an established positive control for inducing apoptosis through active caspase 3. Caspase 3 activity was then determined by adding either extra cellular Annexin V fluorescence detection reagent (Sartorius, 4642) or NucView 488 Active caspase 3 fluorescence detection agent (Biotium, 30029) and monitoring of fluorescence activity was performed by placing the plate in an Incucyte SX5 (Sartorius), incubator dwelling live cell phase/fluorescence microscopy apparatus. Treatments were assayed in technical quadruplicate, and two 10× images were obtained per well at 2 h time intervals starting 2 h post-nanoparticle treatment. Images were analyzed for fluorescence area and intensity using Incucyte Software (2023A, Rev2) and the Basic Analyzer module.

2.2.4. Animal experiments. All experiments were conducted in accordance with the guidelines and protocols approved by the Institutional Animal Care and Use Committee of Oregon Health and Science University (IP00001707). BALB/c mice, APOE$^{-/-}$ KO mice, and C57BL/6 mice were procured from The Jackson Laboratory (Bar Harbor, ME).

2.2.4.1. In vivo transfection after intravenous injection. In vivo transfection experiments were performed in BALB/c mice (5–7 weeks old, 20–25 g, female) or APOE$^{-/-}$ KO mice (5–7 weeks old, 20–25 g, female) after intravenous injection. Briefly, the mice were anesthetized using isoflurane and then injected intravenously (retro-orbitally, 100 µL) with Chol LNPs, GA–Chol LNPs or 20% GA–Chol LNPs, each containing a total dose of 2 µg per mouse of FLuc–mRNA. After 5 h, the mice were injected intraperitoneally with 200 µL of a 15 mg mL^{-1} solution of D-luciferin, followed by imaging using an *In Vivo* Imaging System (IVIS, PerkinElmer).

2.2.4.2. In vivo transfection after intramuscular injection. Briefly, the BALB/c mice (5–7 weeks old, 20–25 g, female) were anesthetized using isoflurane and injected intramuscularly (right thigh muscles of the hind limb, 20 µL) with Chol LNPs, GA–Chol LNPs or 20% GA–Chol LNPs with a total dose of 1 µg per mouse of FLuc–mRNA. After 5 h, the mice were injected intraperitoneally with 200 µL of a 15 mg mL^{-1} solution of D-luciferin, followed by imaging under an *In Vivo* Imaging System (IVIS, PerkinElmer).

2.2.4.3. In vivo transfection after intratumoral injection. To develop various tumors, 4T1 or TUBO cells were injected into the mammary fat pad of the BALB/c mice (5–7 weeks old,

20–25 g, female) at a density of 1×10^5 cells in 100 µL of PBS. MCA205 or Yumm1.7 cells were injected subcutaneously into C57BL/6 mice (5–7 weeks, 20–25 g, female) at a density of 1×10^5 cells in 100 µL of PBS. The mice were observed for 7 days to monitor tumor growth.

Furthermore, tumor-bearing mice were anesthetized using isoflurane and injected intratumorally with 20 µL of either Chol LNPs or GA–Chol LNPs, containing a total dose of 1–2 µg of FLuc–mRNA per mouse. After 5 h, the mice were injected intraperitoneally with 200 µL of a 15 mg mL^{-1} solution of D-luciferin, followed by imaging under an *In Vivo* Imaging System (IVIS, PerkinElmer). For tissue distribution, the mice were perfused with 1× PBS, and the tumor and liver were harvested and imaged under an *In Vivo* Imaging System (IVIS, PerkinElmer).

2.2.4.4. In vivo efficacy study. Briefly, at Day 0, the BALB/c mice (5–7 weeks, 20–25 g, female) were anesthetized using isoflurane, and Luc2-tdTomato-4T1 cells at a density of 1.25×10^6 cells in 100 µL of PBS were injected into the fourth mammary fat pad, which is located near the inguinal area, underneath the nipple. The mice were kept under standard conditions and observed for tumor growth using an *In Vivo* Imaging System (IVIS). On days 8, 11, and 14, the mice were injected intratumorally with either 20 µL of PBS, EGFP mRNA GA–Chol LNPs, or caspase-3 mRNA GA–Chol LNPs, with a total dose of 2 µg per mouse. The mice were observed for total body weight, and tumor growth was monitored using IVIS imaging at weekly intervals. On day 21, the mice were sacrificed, and the tumor was harvested.

3. Results and discussion

3.1. Synthesis and characterization of GA–Chol

GA–Chol was synthesized using a two-step reaction, as shown in Fig. 1a. The intermediate dimethyl (S)-2-isocyanatopentane-dioate (**2**) was obtained as a colorless oil (70% yield). The ^{1}H NMR (400 MHz, CDCl$_3$) and ^{13}C NMR (100 MHz, CDCl$_3$) spectra are shown in SI Fig. 1a and b, respectively. The dimethyl (S)-2-isocyanatopentanedioate (**2**) was subsequently reacted with cholesterol to obtain glutamate–cholesterol (GA–Chol) (**3**) as a colorless crystal (35% Yield). The ^{1}H NMR (400 MHz, CDCl$_3$) and ^{13}C NMR (100 MHz, CDCl$_3$) spectra are shown in SI Fig. 1c and d, respectively.

3.2. LNPs preparation and characterization

The LNPs were prepared by mixing an ethanol phase containing D-Lin–MC3–DMA/DSPC/Chol/DMG–PEG2k with a mol% ratio of 50/10/38.5/1.5, respectively (Fig. 1b), with mRNA in the citrate buffer (25 mM, pH 4.0) using a microfluidic device (Fig. 1c). For GA–Chol LNPs, the GA–Chol was added in the aqueous phase with FLuc mRNA (Fig. 1c) due to its hydrophilic property. The LNPs showed a hydrodynamic diameter of <100 nm; however, the GA–Chol LNPs were significantly larger in size than the Chol LNPs (Fig. 1d). The polydispersity index (PDI) of the LNPs was <0.3 (Fig. 1e), and the zeta potential ranged from −1 mV to −20 mV (Fig. 1f). The GA–Chol LNPs

had significant negative charge, possibly due to the –COOH groups of glutamic acid. The encapsulation efficiency of both LNPs was >90% (Fig. 1g).

3.3. GA–Chol LNPs outperform Chol LNPs *in vitro*

HeLa and HEK293T cells were treated with 50 ng, 100 ng, and 200 ng of FLuc mRNA containing Chol LNPs or GA–Chol LNPs, and transfection was evaluated based on luciferase expression. The GA–Chol LNPs showed approximately 20-fold and 10-fold higher luciferase expression than Chol LNPs in HeLa and HEK293T cells, respectively, at a 200 ng FLuc mRNA dose (Fig. 2a). It has already been reported that the cholesterol derivative can influence the transfection efficiency of LNPs by improving cellular uptake.[18,19,21] Moreover, according to the toxicity data, both Chol and GA–Chol LNPs showed minimal toxicity at 50 ng, 100 ng, and 200 ng FLuc mRNA doses in both HeLa and HEK293T cell lines (Fig. 2b).

The endosomal escape of Chol and GA–Chol LNPs was carried out in the HEK293T–Gal8–GFP cell line, as reported earlier.[19] HEK293T–Gal8–GFP cells feature a Galectin 8-GFP reporter system, enabling the visualization of endosome destabilization—a hallmark of endosomal damage—through GFP puncta. The cells were treated with 200 ng of FLuc mRNA containing Chol or GA–Chol LNPs, and after 24 h of treatment, Gal8 recruitment was evaluated using confocal microscopy (Leica DMi8, Leica Microsystems). As shown in Fig. 2c, the GFP puncta were visualized with both LNPs. However, there

was no significant difference in the endosomal escape of Chol and GA–Chol LNPs.

3.4. Chol and GA–Chol LNPs are APOE dependent after systemic administration

The Chol and GA–Chol LNPs were injected in BALB/c mice ($n = 2$) *via* retro-orbital injection with a total dose of 2 µg FLuc mRNA per mouse. The IVIS images were taken 5 h after injection. Fig. 3a and b demonstrate the capability of both Chol and GA–Chol LNPs for liver transfection. However, the GA–Chol LNPs showed lower transfection than the Chol LNPs. This could be attributed to the fact that the GA–Chol has physicochemical properties that differ from those of cholesterol. As we observed, the GA–Chol LNPs have a significantly higher negative charge compared to the Chol LNPs, which could potentially modulate the protein binding (APOE) of LNPs *in vivo* after systemic administration. Similar findings have been reported by Radmand *et al.*, who screened cationic cholesterol and stated that cholesterol derivatives can lead to tissue tropisms different from those of cholesterol or other membrane lipids.[8] Moreover, the low liver transfection efficiency of GA–Chol LNPs may be attributed to their rapid clearance after systemic circulation and their lower affinity for hepatocytes.[16]

Next, we utilized APOE KO^{−/−} mice as LNP recipients to understand the mechanism of Chol and GA–Chol LNPs hepatic accumulation after intravenous administration. Generally, after systemic administration, LNPs undergo protein corona formation on their surface *via* hydrophobic
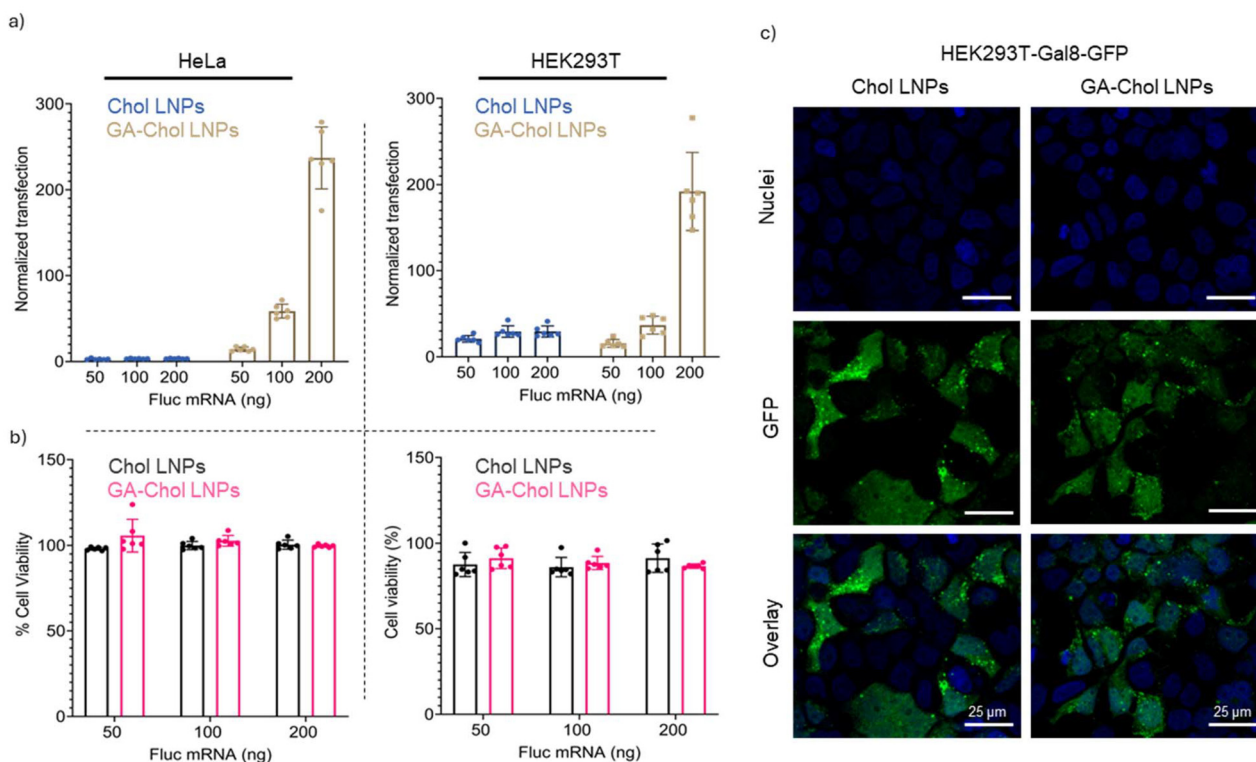

Fig. 2 *In vitro* evaluation of Chol and GA–Chol LNPs: (a) transfection efficiency and (b) cytotoxicity at 50 ng, 100 ng, and 200 ng of FLuc mRNA in HeLa and HEK293T cells ($n = 6$) after 24 h, (c) endosomal escape in HEK293T–Gal8–GFP cells at 200 ng FLuc mRNA after 24 h ($n = 3$).
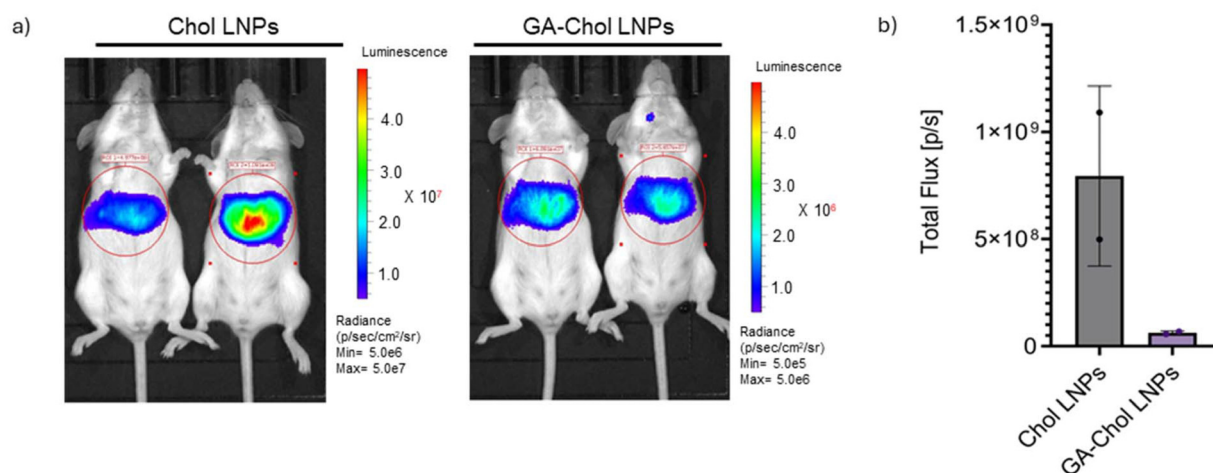
Fig. 3 *In vivo* evaluation of Chol and GA−Chol LNPs in BALB/c mice ($n = 2$): (a) 6 h IVIS images, (b) total flux (p/s) after 2 μg of FLuc mRNA injected retro-orbitally.
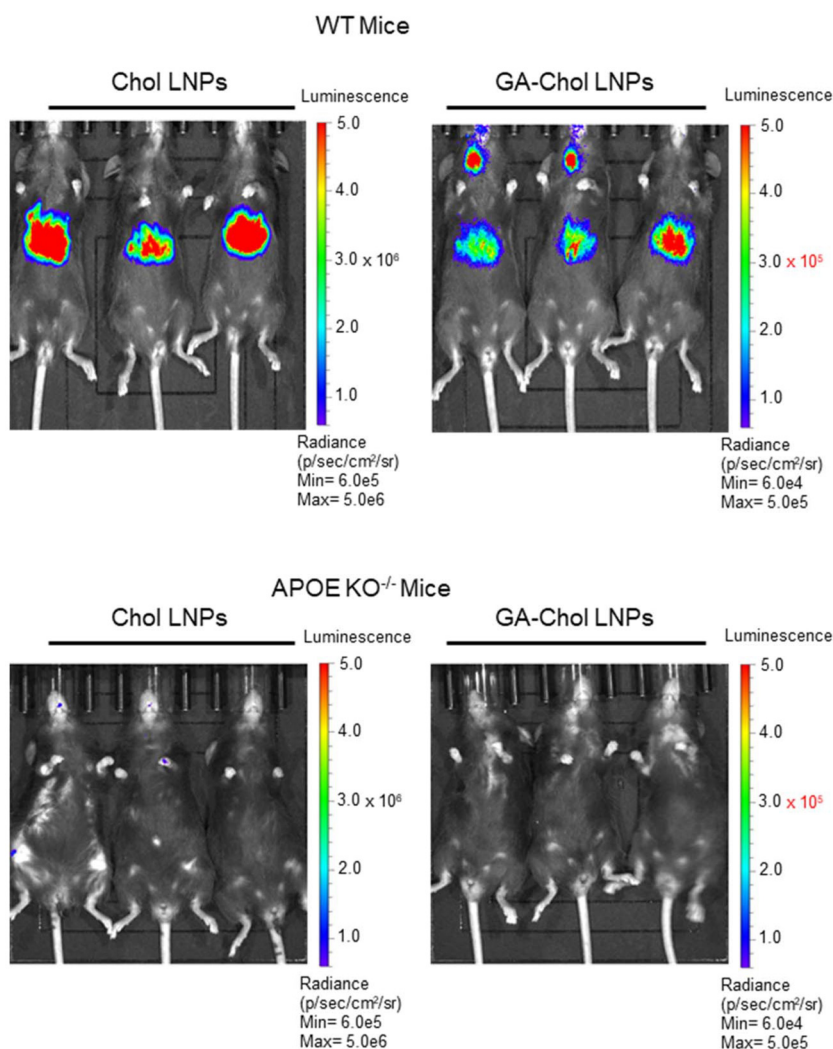

Fig. 4 *In vivo* transfection of Chol LNPs and GA−Chol LNPs in WT mice and APOE KO$^{-/-}$ mice ($n = 3$) 5 h after retro-orbital injection with a total dose of 2 μg of FLuc mRNA.

interactions, with a significant component of the protein corona frequently composed of the protein Apolipoprotein E (APOE). Apolipoproteins are a class of proteins involved in the endogenous organization and formation of cholesterol-carrying lipid micelles in the body, playing a key role in trafficking cholesterol and other lipids throughout the body through receptor-mediated endocytosis. It has been previously reported that the APOE protein facilitates the internalization of LNP in hepatocytes *via* the LDLR.[9–11] In alignment with previously reported observations, injection of APOE KO$^{-/-}$ mice with either Chol or GA–Chol LNPs with 2 µg FLuc mRNA intravenously showed no transfection in the liver 5 h post-injection Fig. 4. This confirms the APOE dependency of both LNPs for effective transfection following intravenous administration.

Since it has been reported that neutrally charged nanoparticles show increased ApoE binding after systemic administration, and GA–Chol LNPs are strongly negatively charged, this may explain their lower liver tropism.[22] Therefore, to examine whether lowering GA–Chol content influences charge and liver tropism due to increased ApoE binding, we reduced GA–Chol content to 20 mol% (SI Fig. S2a), with LNP characteristics shown in SI Fig. S3b and c. It was found that the 20% GA–Chol LNPs did not show a significant change in charge (-12.5 ± 1.9 mV) (SI Fig. S3d). However, interestingly, 20% GA–Chol LNPs exhibited improved liver targeting after intramuscular (SI Fig. S2e) and retro-orbital injections (SI Fig. S2f). This may be due to a change in surface properties of the LNPs caused by an increase in membrane lipid (DSPC), which was 28.5 mol% in 20% GA–Chol LNPs.
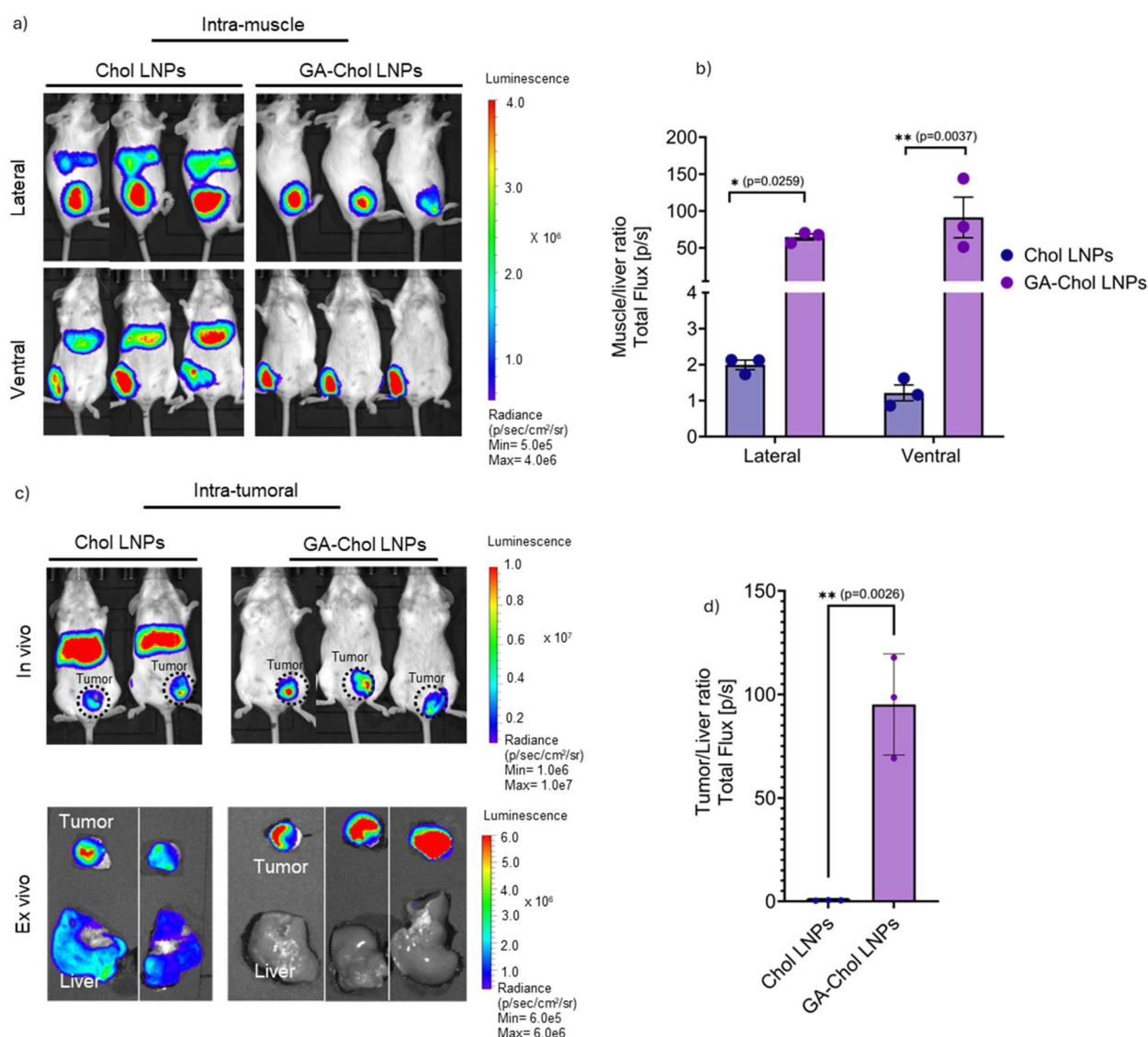

Fig. 5 *In vivo* transfection of Chol LNPs and GA−Chol LNPs. (a) IVIS images of BALB/c mice 5 h after intramuscular injection with 1 µg FLuc mRNA dose, (b) muscle/liver ROI ratio, and (c) IVIS images of 4T1 tumor-bearing BALB/c mice after intratumoral injection with 1 µg FLuc mRNA dose, (d) tumor/liver ROI ratio. All the data are presented (n = 3) as mean $\pm$ SD and analyzed using Student's t-test or two-way ANOVA followed by Šídák's multiple comparisons test, wherein $p < 0.05$ is considered statistically significant (*$p \leq 0.05$, **$p \leq 0.005$).

3.5. GA–Chol LNPs showed localized transfection after intramuscular and intratumoral injection

Previous studies have shown that LNPs often leak into the systemic circulation after intramuscular injection, which can lead to off-target hepatotoxicity.[12–16] Here, we injected Chol and GA–Chol LNPs into BALB/c mice intramuscularly with a total FLuc mRNA dose of 1 μg and imaged them using an IVIS after 5 h. As shown in Fig. 5a, the Chol LNPs were able to leak into the systemic circulation and exhibited liver and muscle transfection. On the other hand, GA–Chol LNPs transfected the muscle with minimal transfection in the liver. The mice were imaged from both lateral and ventral positions. The ROI quantification showed that the muscle-to-liver ratio of Chol-

LNPs was >50-fold less than that of GA–Chol (lateral, *p = 0.0259; ventral, **p = 0.0037) (Fig. 5b). Similarly, as shown in Fig. 5c, the Chol LNPs injected intratumorally leaked in the systemic circulation and transfected the liver as well. In contrast, the GA–Chol LNPs showed localized transfection in the tumor only. As per the ROI quantification, the tumor-to-liver ratio of GA–Chol LNPs was >80-fold in comparison to the Chol LNPs (**p = 0.0026) (Fig. 5d). In support of these results, Kawaguchi *et al.* have already shown the impact of cholesterol on liver transfection by varying the mol% ratio of cholesterol from 10 to 40%. They observed that the liver transfection rate after intramuscular injection of LNPs was directly proportional to the amount of cholesterol (mol%) in the formulation. They stated that after intramuscular administration of mRNA–LNP,
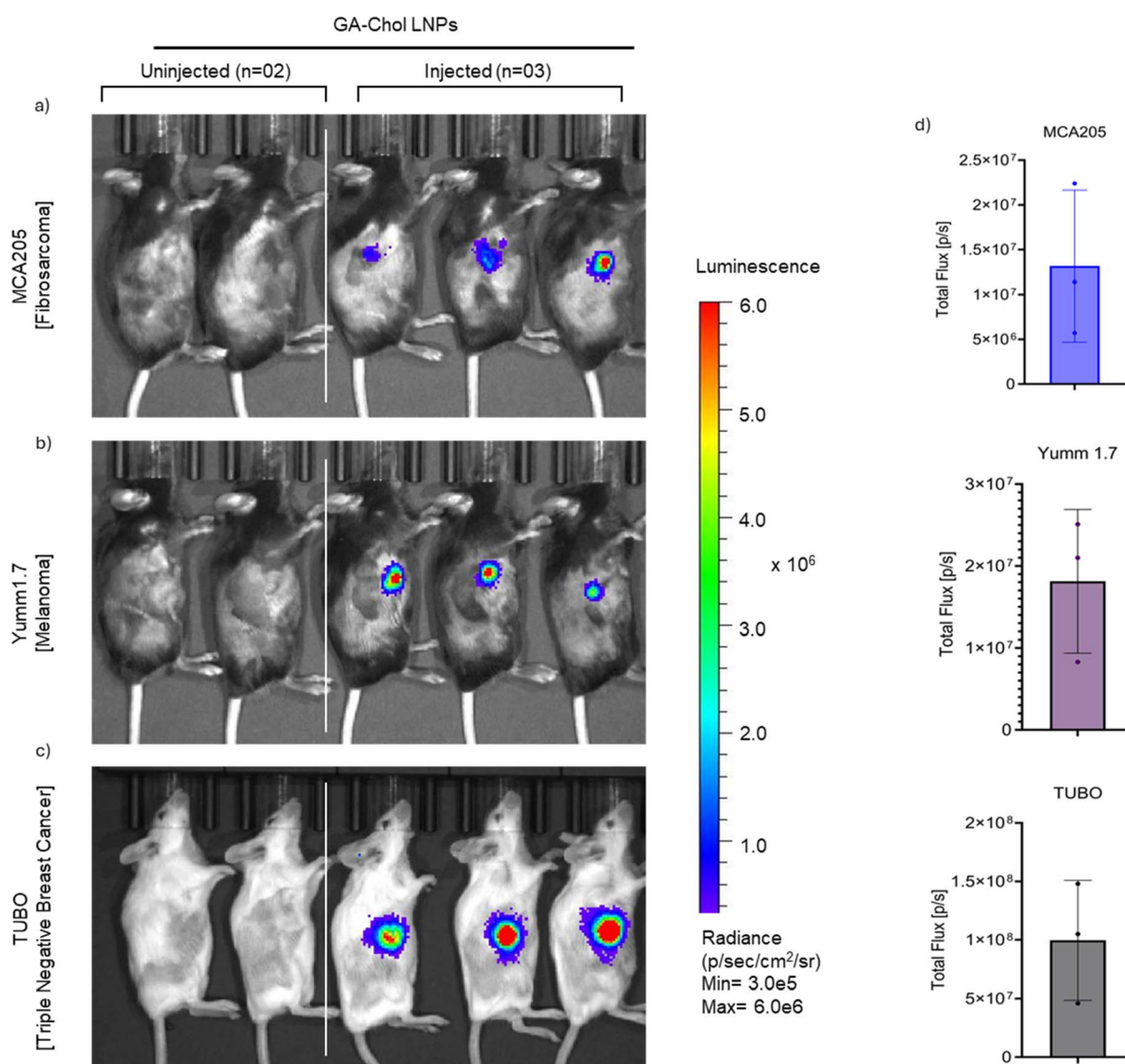

Fig. 6 Evaluation of the consistency of GA–Chol LNPs across different xenograft cancer models. IVIS images of (a) fibrosarcoma, (b) melanoma, and (c) triple negative breast tumor-bearing C57BL/6 or BALB/c mice 5 h after intratumoral injection with a total dose of 1 μg of FLuc–mRNA, and (d) ROI plotted for different tumors.

the cholesterol (mol%) of mRNA–LNP can be degraded in the systemic circulation, thereby decreasing its protein expression in the liver.[16] Since GA–Chol is a new chemical entity with different physicochemical properties than cholesterol, it may follow a similar mechanism to low mol% cholesterol in LNPs and show localized transfection.

3.6. GA–Chol LNPs showed consistent localized transfection in various tumor types *in vivo*

The consistency of GA–Chol LNPs in terms of localized transfection after intratumor injection was determined in a diverse selection of murine tumor cell line models, namely MCA205 (fibrosarcoma), Yumm1.7 (melanoma), and TUBO (triple-negative breast cancer). After 7 days post-tumor inoculation, GA–Chol LNPs with 1 μg of FLuc mRNA were injected intratumorally, and bioluminescence imaging was performed after 5 h. As shown in Fig. 6a–c, the GA–Chol LNPs demonstrated localized transfection in all tumor types. Overall, this confirms the consistency of GA–Chol LNPs for localized transfection when injected intratumorally.

3.7. Caspase-3 mRNA shows caspase-3 activity

In homeostasis, cells are programmed to survive, proliferate, or die, and this process is controlled *via* complex intracellular pathways. Caspases are a family of cysteine proteases present in an inactive form in all animal cells. Once activated, they attain proteolytic activity, utilizing a cysteine side chain to catalyze peptide bond cleavage at aspartyl residues in their substrates. The name caspase denotes their function: cysteine-dependent ASPartyl-specific proteASE.[23] Different caspases are linked to each other and act as signal transduction proteins, altering the activity of a diverse repertoire of proteins, including enzymes such as endonucleases that degrade cellular DNA, as well as lipid flippases and scramblases. Caspase-3 is a crucial protease involved in apoptosis, the process of programmed cell death. It acts as an "executioner caspase", meaning it's primarily responsible for cleaving other proteins and ultimately initiating cellular disassembly and apoptosis.[24,25] With the purpose of utilizing constitutively activated (CA) caspase-3 mRNA to cause tumor cell death *in vivo*, we first evaluated *in vitro* caspase 3 activity after CA–Casp 3 mRNA administration in the 4T1 tumor cell line. With lipid scramblases being established targets of active caspase 3 activity, we utilized an extracellular Annexin V fluorescence detection reagent to enable the visualization of Phosphatidyl Serine accumulation on the surface of mRNA-treated cells. Likewise, we utilized a fluorescent probe containing a caspase 3 recognized peptide that, when cleaved by caspase 3, results in bright nuclear fluorescence (NucView 488 Active caspase 3 fluorescence detection agent (Biotium, 30029)). Utilizing
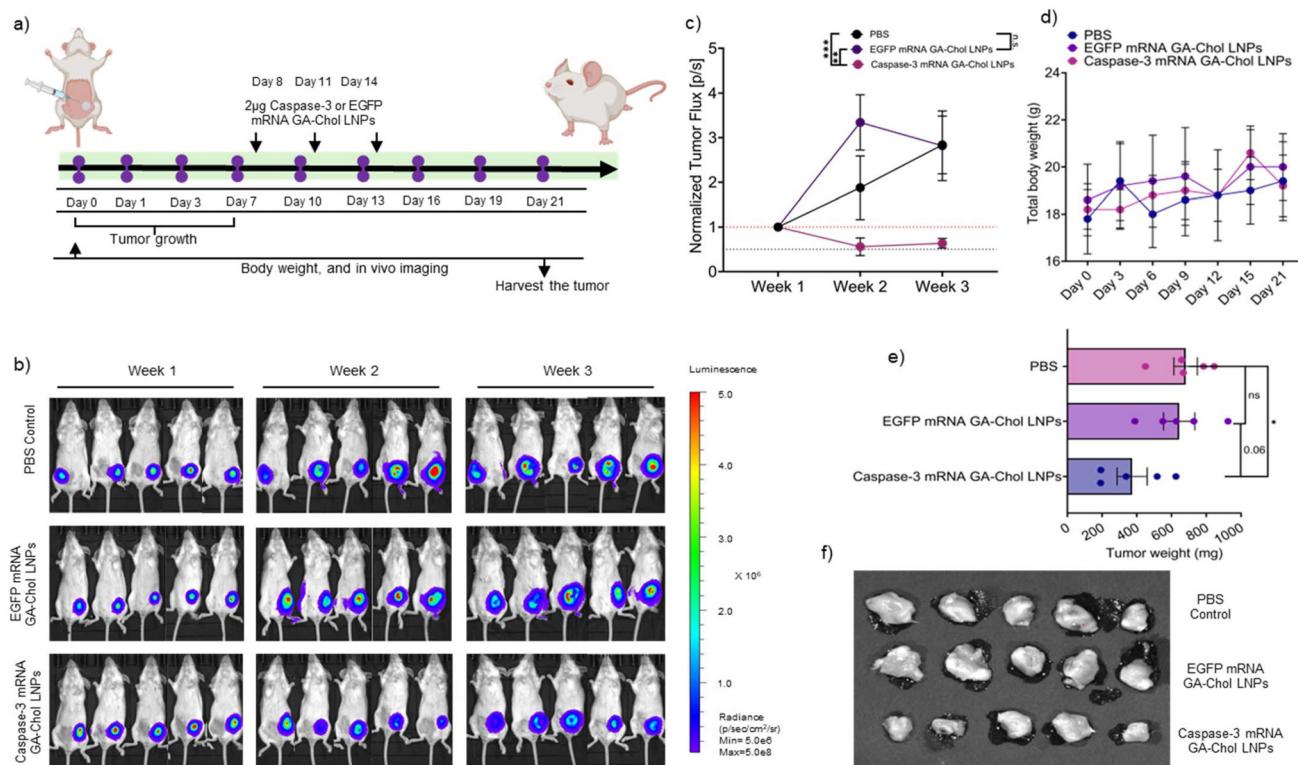

Fig. 7 *In vivo* efficacy study of GA–Chol LNPs encapsulated with caspase-3 mRNA in Luc2-tdTom-4T1 tumor-bearing BALB/c mice ($n = 5$). (a) Tumor implantation and treatment layout, (b) IVIS images of mice after week 1 (prior treatment), week 2, and week 3, (c) ROI of tumor growth after week 1 (prior treatment), week 2, and week 3, (d) total body weight of mice throughout the studies, (e) total weight of the tumor after day 21, and (f) IVIS brightfield images of harvested tumor on last day of the study. All data are presented as mean ± SEM and analyzed using an unpaired *t*-test or two-way ANOVA mixed-effects analysis, wherein $p < 0.05$ is considered statistically significant (*$p \leq 0.05$, **$p \leq 0.005$, ***$p \leq 0.0005$).

Staurosporine (100 ng per well) as a well-established, robust, caspase 3-inducing cell death agent for a positive control, we monitored fluorescence intensity over time to validate the CA–Casp3 mRNA construct. As shown in SI Fig. S3a and S3b, we observed significantly elevated caspase-3 activity (as indicated by Annexin V positivity and NucView 488 positivity) beginning at 2 h post-LNP treatment for the 50 and 100 ng GA–Chol caspase-3 LNPs treatment compared to GA–Chol LNPs containing equivalent amounts of mRNA encoding Firefly Luciferase (Luc) or PBS controls. Importantly, the Staurosporine positive controls likewise demonstrated rapid and significant increases in fluorescence activity, validating the assay and thus confirming the activity of the CA–Casp3 mRNA construct.

3.8. Caspase-3 mRNA encapsulated GA–Chol LNPs slow down tumor growth *in vivo*

To assess the *in vivo* efficacy of combining the CA–Casp3 construct with the tumor retentive GA–Chol LNP, Luc2-tdTomato 4T1 murine breast tumors were implanted orthotopically in BALB/c mice and subsequently injected with either FLuc GA–Chol LNPs or caspase-3 GA–Chol LNPs with a total dose of 2 µg per mouse intratumorally at days 8, 12, and 15 (Fig. 7a). An equal volume of PBS was injected as a negative control. IVIS imaging before and after injection showed tumor growth pattern (Fig. 7b). Mice treated with caspase-3 GA–Chol LNPs showed an initial reduction in tumor size followed by cessation of tumor growth, in contrast to the continual tumor growth observed in either PBS control (***$p < 0.005$) or FLuc GA–Chol LNPs (**$p < 0.05$) (Fig. 7c). The total body weight of mice over the treatment time did not show any significant change. The weight (mg) of the tumor harvested on Day 21 was significantly lower (*$p < 0.05$) in animals treated with caspase-3 GA–Chol LNPs compared to those treated with PBS. While trending consistently with observed reduced luciferase expression, we observed decreased overall tumor weight difference in CA–caspase-3 GA–Chol LNP compared to FLuc GA–Chol LNPs; however, this comparison did not reach statistical significance ($p = 0.06$) (Fig. 7d). Variation in starting tumor weight, as well as retention of non-tumor stromal constituents (*i.e.*, endothelial cells, extracellular matrix proteins, immune cells) may be responsible for the lack of achieving end point tumor mass statistical significance ($p < 0.05$). Fig. 7e shows IVIS images of the harvested tumor. The caspase-3 mRNA did not result in complete gross tumor regression, but significantly reduced initial tumor mass and slowed overall tumor growth. These data demonstrate proof of concept for employing GA–Chol LNPs for the local administration of therapeutic anticancer mRNA that could otherwise be systemically detrimental.

4. Conclusions

LNPs are one of the most advanced drug delivery systems for nucleic acids, and their translational potential is evident in FDA-approved LNP formulations of the mRNA vaccine. However, LNPs are currently limited in application due to

hepatic tropism. Frequently, after local injections, LNPs leak into systemic circulation and both accumulate and release cargo into the liver, resulting in systemic cargo expression and hepatic inflammation. In circumstances such as prophylactic antibody-mediated vaccination, only low-dose LNPs are required to achieve therapeutic responses, limiting concerns of hepatotoxicity. In fact, either hepatic or injection site inflammation caused by LNP components acts as an essential adjuvant for engaging and educating the antibody-mediated adaptive immune response.[26] However, in circumstances where therapeutic results require increased levels of nucleic acid delivery (*i.e.*, therapeutic gene replacement), concomitant increases in LNP constituents could result in unacceptable levels of hepatotoxicity. Furthermore, local expression of mRNA products, rather than systemic dissemination, could allow for the administration of potentially systemically detrimental genetically encoded cargo or achieve increases in therapeutic efficacy by enabling transient, local high concentrations of expressed cargo, as has been demonstrated necessary for the effective generation of cytotoxic T cell vaccines.[27] Consequently, there are numerous efforts from the LNP research community to achieve more efficient and extrahepatic LNP delivery and nucleic acid cargo expression.[28–31] Most commonly, tissue delivery and specific expression are explored by altering cationic lipids and modifying the external-facing PEG moiety.

Our present study demonstrates that a synthetic cholesterol derivative, namely GA–Chol, facilitates the retention of LNPs at the local site by preventing leakage in systemic circulation. This corroborates evidence that other cholesterol derivatives or alternatives, such as GA–Chol, may also show an advantage in reducing off-target liver delivery, as well as associated LNP toxicities. Moreover, we have demonstrated that the GA–Chol LNPs are feasible for therapeutic applications through intratumoral injections in the 4T1 breast cancer model. This begins to set the stage for further consideration in clinical employment of such LNPs for unresectable, therapeutic non-responsive cancers, including advanced colorectal and breast tumors, as well as sarcoma. The enhanced efficacy of GA–Chol LNPs in increasing mRNA-delivered antigenic responses by cytotoxic T cells, as well as their suitability for local DNA delivery, are intriguing implications of this work and are currently under preliminary investigation.

Conflicts of interest

G. S. is a co-founder of EnterX Bio and has an advisory role to Rare Air Inc., Serina Tx, and Mana Bio.

Data availability

The data that support the findings of this study are available from the corresponding author upon reasonable request.

Supplementary information is available. Fig. S1. ^{1}H NMR and ^{13}C NMR.

Fig. S2. Impact of lower amount (20 mol%) of GA-Chol on *in vivo* transfection.

Fig. S3. *In vitro* evaluation of Caspase-3 mRNA activity in 4T1 cells.

Table S1. List of published research showing liver tropism of LNPs after local injections. See DOI: https://doi.org/10.1039/d5pm00166h.

Acknowledgements

References

1 X. Hou, *et al.*, Lipid nanoparticles for mRNA delivery, *Nat. Rev. Mater.*, 2021, **6**(12), 1078–1094.

2 Ü. F. Aydın and A. Tuli, Lipid-Based Nanocarriers and Applications in Medicine, in *Recent Progress in Pharmaceutical Nanobiotechnology: A Medical Perspective*, 2023, vol. 8, pp. 25–56.

3 Y. Jia, *et al.*, Lipid nanoparticles optimized for targeting and release of nucleic acid, *Adv. Mater.*, 2024, **36**(4), 2305300.

4 C. H. Albertsen, *et al.*, The role of lipid components in lipid nanoparticles for vaccines and gene therapy, *Adv. Drug Delivery Rev.*, 2022, **188**, 114416.

5 Y. Liu, *et al.*, Corosolic acid derivative-based lipid nanoparticles for efficient RNA delivery, *J. Controlled Release*, 2025, **378**, 1–17.

6 K. Swetha, *et al.*, Recent advances in the lipid nanoparticle-mediated delivery of mRNA vaccines, *Vaccines*, 2023, **11**(3), 658.

7 G. Sahay, *et al.*, Efficiency of siRNA delivery by lipid nanoparticles is limited by endocytic recycling, *Nat. Biotechnol.*, 2013, **31**(7), 653–658.

8 A. Radmand, *et al.*, Cationic cholesterol-dependent LNP delivery to lung stem cells, the liver, and heart, *Proc. Natl. Acad. Sci. U. S. A.*, 2024, **121**(11), e2307801120.

9 M. Hosseini-Kharat, K. E. Bremmell and C. A. Prestidge, Why Do Lipid Nanoparticles Target the Liver? Understanding of Biodistribution and Liver-Specific Tropism, *Mol. Ther.–Methods Clin. Dev.*, 2025, **33**(1), 101436.

10 F. Sebastiani, *et al.*, Apolipoprotein E binding drives structural and compositional rearrangement of mRNA-containing lipid nanoparticles, *ACS Nano*, 2021, **15**(4), 6709–6722.

11 N. Saber, M. E. Senti and R. M. Schiffelers, Lipid nanoparticles for nucleic acid delivery beyond the liver, *Hum. Gene Ther.*, 2024, **35**(17–18), 617–627.

12 J. Di, *et al.*, Biodistribution and non-linear gene expression of mRNA LNPs affected by delivery route and particle size, *Pharm. Res.*, 2022, **39**(1), 105–114.

13 N. Pardi, *et al.*, Expression kinetics of nucleoside-modified mRNA delivered in lipid nanoparticles to mice by various routes, *J. Controlled Release*, 2015, **217**, 345–351.

14 J. Chen, *et al.*, Combinatorial design of ionizable lipid nanoparticles for muscle-selective mRNA delivery with minimized off-target effects, *Proc. Natl. Acad. Sci. U. S. A.*, 2023, **120**(50), e2309472120.

15 M. J. Carrasco, *et al.*, Ionization and structural properties of mRNA lipid nanoparticles influence expression in intramuscular and intravascular administration, *Commun. Biol.*, 2021, **4**(1), 956.

16 M. Kawaguchi, *et al.*, Effect of cholesterol content of lipid composition in mRNA-LNPs on the protein expression in the injected site and liver after local administration in mice, *J. Pharm. Sci.*, 2023, **112**(5), 1401–1410.

17 EMA, *Assessment Report Comirnaty. Procedure No. EMEA/H/C/005735/0000*, European Medicines Agency, Netherlands, 2021.

18 S. Patel, *et al.*, Naturally-occurring cholesterol analogues in lipid nanoparticles induce polymorphic shape and enhance intracellular delivery of mRNA, *Nat. Commun.*, 2020, **11**(1), 983.

19 M. Herrera, *et al.*, Illuminating endosomal escape of polymorphic lipid nanoparticles that boost mRNA delivery, *Biomater. Sci.*, 2021, **9**(12), 4289–4300.

20 Y. Eygeris, *et al.*, Deconvoluting lipid nanoparticle structure for messenger RNA delivery, *Nano Lett.*, 2020, **20**(6), 4543–4549.

21 S. Patel, *et al.*, Boosting intracellular delivery of lipid nanoparticle-encapsulated mRNA, *Nano Lett.*, 2017, **17**(9), 5711–5718.

22 A. Akinc, *et al.*, Targeted delivery of RNAi therapeutics with endogenous and exogenous ligand-based mechanisms, *Mol. Ther.*, 2010, **18**(7), 1357–1364.

23 B. Howley and H. Fearnhead, Caspases as therapeutic targets, *J. Cell. Mol. Med.*, 2008, **12**(5a), 1502–1516.

24 H. Y. Chang and X. Yang, Proteases for cell suicide: functions and regulation of caspases, *Microbiol. Mol. Biol. Rev.*, 2000, **64**(4), 821–846.

25 S. Fulda, *et al.*, Cellular stress responses: cell survival and cell death, *Int. J. Cell Biol.*, 2010, **2010**(1), 214074.

26 M.-G. Alameh, *et al.*, Lipid nanoparticles enhance the efficacy of mRNA and protein subunit vaccines by inducing robust T follicular helper cell and humoral responses, *Immunity*, 2021, **54**(12), 2877–2892.

27 M. A. Burchill, *et al.*, T cell vaccinology: exploring the known unknowns, *Vaccine*, 2013, **31**(2), 297–305.

28 K. Y. Vlasova, Synthesis of ionizable lipopolymers using split-Ugi reaction for pulmonary delivery of various size RNAs and gene editing, *Nat. Commun.*, 2025, **16**(1), 4021.

29 M. Kim, *et al.*, Dual SORT LNPs for multi-organ base editing, *Nat. Biotechnol.*, 2025, 1–9.

30 E. L. Han, *et al.*, Peptide-Functionalized Lipid Nanoparticles for Targeted Systemic mRNA Delivery to the Brain, *Nano Lett.*, 2024, **25**(2), 800–810.

31 M. Jester, *et al.*, Ionizable lipid nanoparticles with functionalized PEG-lipids increase retention in the tumor microenvironment, *Mol. Ther.–Methods Clin. Dev.*, 2025, **33**(2), 101457.